Adipokinetic hormone signaling mediates the fecundity of *Diaphorina citri* infected by '*Candidatus* Liberibacter asiaticus'

Jiayun Li[1], Paul Holford[3], George Andrew Charles Beattie[3], Shujie Wu[1], Jielan He[1], Shijian Tan[1], Desen Wang[1], Yurong He[1], Yijing Cen[1]*, Xiaoge Nian[1,2]*

[1]National Key Laboratory of Green Pesticide, Department of Entomology, College of Plant Protection, South China Agricultural University, Guangzhou, 510642, China；

[2]Henry Fok School of Biology and Agriculture, Shaoguan University, Shaoguan, 512005, China；

[3]School of Science, Western Sydney University, Locked Bag 1797, Penrith, NSW 2751, Australia;

*Corresponding author: Yijing Cen and Xiaoge Nian

Email: cenyj@scau.edu.cn; nianxiaoge@scau.edu.cn

Abstract

Diaphorina citri is the primary vector of the bacterium, '*Candidatus* Liberibacter asiaticus' (*C*Las) associated with the severe Asian form of huanglongbing. *C*Las-positive *D. citri* are more fecund than their *C*Las-negative counterparts and require extra energy expenditure. Therefore, understanding the molecular mechanisms linking metabolism and reproduction is of particular importance. In this present study, we found adipokinetic hormone (*DcAKH*) and its receptor (*DcAKHR*) were essential for increased lipid metabolism and fecundity in response to *C*Las infection in *D. citri.* Knockdown of *DcAKH* and *DcAKHR* not only resulted in triacylglycerol accumulation and a decline of glycogen, but also significantly decreased fecundity and *C*Las titer in ovaries. Combined *in vivo* and *in vitro* experiments showed that miR-34 suppresses *DcAKHR* expression by binding to its 3' untranslated region, whilst overexpression of miR-34 resulted in a decline of *DcAKHR* expression and *C*Las titer in ovaries and caused defects that mimicked *DcAKHR* knockdown phenotypes. In addition, knockdown of *DcAKH* and *DcAKHR* significantly reduced juvenile hormone (JH) titer and JH signaling pathway genes in fat bodies and ovaries, including the JH receptor, *methoprene-tolerant* (*DcMet*), and the transcription factor, *Krüppel homolog 1 (DcKr-h1)*, that acts downstream of it, as well as the egg development related genes *vitellogenin 1-like* (*DcVg-1-like*), *vitellogenin A1-like* (*DcVg-A1-like*) and the vitellogenin receptor (*DcVgR*). As a result, *C*Las hijacks AKH/AKHR-miR-34-JH signaling to improve *D. citri* lipid metabolism and fecundity, while simultaneously increasing the replication of *C*Las, suggesting a mutualistic interaction in *D. citri* ovaries with *C*Las.

Key words: huanglongbing; *Diaphorina citri*; *DcAKH*/*DcAKHR*; miR-34; mutualism

Introduction

The majority of devastating plant pathogens, including viruses and bacteria, are transmitted by insect vectors [1]. In recent decades, the interactions between vectors and pathogens have been widely studied [1-4]. However, studies on the mechanisms underlying these interactions have mainly focused on vector-virus or vector-fungus interactions; less research has been performed on vector-bacteria interactions. Knowledge of the relationships between vectors and pathogens is of great significance for understanding the epidemiology of plant pathogens, and this knowledge may help develop new strategies for controlling both vectors and pathogens. The severe Asian form of huanglongbing (HLB) is currently the most destructive citrus disease in Asia and the Americas where it is associated with the phloem-restricted, Gram-negative, α–Proteobacteria '*Candidatus* Liberibacter asiaticus' (*C*Las) and transmitted by the Asian citrus psyllid, *Diaphorina citri* Kuwayama (Hemiptera: Psyllidae) [5-9]. However, since *C*Las has not been cultured *in vitro,* Koch's postulates have not been proven. Control of *D. citri* is the most effective way to prevent HLB epidemics [6,7] but experience in Asia [10] and the United States of America [11,12], and recent press reports from Brazil, indicate that it is impossible to suppress psyllid populations with insecticides to levels that prevent spread of *C*Las.

Previous studies have reported that infection with *C*Las significantly increases the fecundity of *D. citri* [13-15]. Reproduction is a costly process in terms of energy usage in the adult life of female insects [16], and there is an inevitable trade-off between lipid storage and use, because animals mobilize their lipid reserves during reproduction. How *D. citri* maintains a balance between lipid metabolism and increased fecundity after infection with *C*Las is not known.

In insects, energy mobilization is under control of adipokinetic hormone (AKH), which was the first insect neurohormone to be identified; it was shown to stimulate lipid mobilization for locomotor activity in locusts [17]. To date, more than 80 different forms of AKH have been identified or predicted in arthropod species due to similar structural characteristics of the enzyme [18]. The mechanisms of synthesis and biological activity of AKH have also been investigated. Insect store lipids in the form of triacylglycerides (TAG) and as carbohydrates in the form of glycogen in their fat bodies [19]. Under conditions of energy demand, AKHs are

67 synthesized in the corpora cardiaca, released into the hemolymph and bind to receptors
68 (AKHRs) located on the plasma membrane of fat body cells. AKHR binding and activation
69 triggers the release of energy-rich substrates after which various cellular signaling pathway
70 components come into play [20]. AKHRs are a class of G protein-coupled receptors and were
71 first identified in *Drosophila melanogaster* [21] and *Bombyx mori* [22]; subsequently, they were
72 identified in a large number of insect species [23-26].

73 Recent studies have shown that AKH/AKHR signaling plays a regulatory role during
74 female reproduction in insects. For example, depletion of AKHR in *Bactrocera dorsalis* resulted
75 in TAG accumulation, decreased sexual courtship activity, and fecundity [27]. AKHR
76 knockdown in *Nilaparvata lugens* interferes with trehalose homeostasis and vitellogenin
77 uptake by oocytes, which causes delayed oocyte development and reduced fecundity [28].
78 AKH/AKHR signaling also regulates vitellogenesis and egg development in *Locusta migratoria*
79 via triacylglycerol mobilization and trehalose homeostasis [29]. As outlined above, the
80 fecundity of *D. citri* is increased by *C*Las. Whether AKH/AKHR signaling participates in this
81 increase in fecundity due to infection via alterations in lipid metabolism is not currently known.

82 Although numerous studies have been conducted on the AKH/AKHR signaling pathway,
83 miRNA-mediated regulation of the AKH signaling pathway at the post-transcriptional level has
84 been little studied. MicroRNAs (miRNAs) are small, non-coding RNAs containing
85 approximately 22 nucleotides that act mostly on the 3' untranslated region (UTR) of target
86 mRNAs, resulting in translation repression or mRNA degradation [30]. miRNAs play important
87 roles in regulating cellular events at the post-transcriptional level during biological processes
88 [30,31,33]. For example, in term of host-virus interactions, miR-8 and miR-429 target *Broad*
89 *isoform Z2*, the gene involved in the hormonal regulation of single nucleopolyhedrovirus
90 (HaSNPV)-mediated climbing behavior in *Helicoverpa armigera* [33]. In relation to
91 reproduction, in *Aedes aegypti*, miR-275 is essential for egg development [34], miR-309 for
92 ovarian development [35] and miR-8 for other reproductive processes [36]. As for lipid
93 metabolism, knockdown of miR-277 in *A. aegypti* activates insulin/FOXO signaling by
94 increasing the expression of ilp7 and ilp8, which reduces TAG levels and inhibits ovarian
95 development [37]. Nevertheless, the functions of the miRNAs in insect-pathogen interactions
96 need further investigation. To date, there are no reports that miRNAs participate in *D.*

97 *citri*-*C*Las interactions or are hijacked by *C*Las to affect lipid metabolism and the fecundity of *D.*
98 *citri*. As a consequence, in this study, we used the *D. citri*-*C*Las system as a model to study the
99 molecular events associated with AKH/AKHR signaling that affect lipid metabolism and
100 increase fecundity of *D. citri* induced by *C*Las. Our study contributes to our understanding of
101 the interactions between vectors and pathogens and may also provide new ways for
102 controlling *D. citri* and HLB.
103

Results

Effects of *C*Las infection on the reproduction and metabolism of adult *D. citri*.

Total TAG and glycogen levels in fat bodies of *C*Las-negative and *C*Las-positive psyllids were determined. After infection with *C*Las, the TAG and glycogen levels of *C*Las-positive psyllids significantly increased compared with *C*Las-negative individuals (Figures 1A-B). Since TAG is mainly stored in fat bodies as lipid droplets, we next evaluated the changes in the lipid droplet size using Nile red staining. As shown in Figure 1C, the size of lipid droplets in the *C*Las-positive group was significantly larger than those of the *C*Las-negative group. In order to evaluate the effects of *C*Las on the reproduction of *D. citri*, the preoviposition period, oviposition period and fecundity of both *C*Las-negative and *C*Las-positive psyllids were examined. After infection with *C*Las, the preoviposition period was significantly shortened, the oviposition period was extended, and the fecundity was markedly increased (Figures 1D-E).

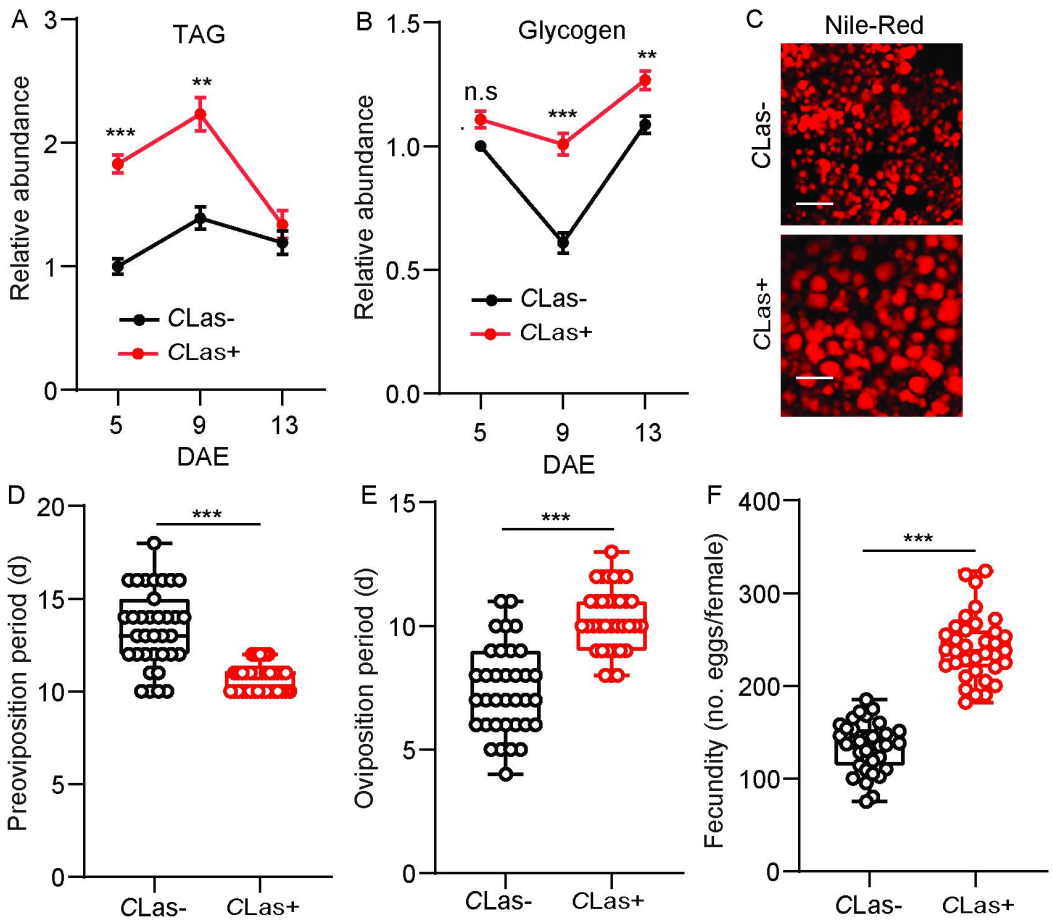

Figure 1. Effects of *C*Las on lipid metabolism and reproductive behavior of *D. citri*.

(A) Comparison of TAG levels in the fat bodies of *C*Las-positive (*C*Las+) and *C*Las-negative

119 (*C*Las-) females 5, 9, 13 days after emergence (DAE). (B) Comparison of glycogen levels in
120 the fat bodies of *C*Las+ and *C*Las- females 5, 9, 13 DAE. (C) Lipid droplets in fat bodies
121 dissected from *C*Las+ and *C*Las- females 9 DAE stained with Nile red. Scale bar = 40 μm.
122 (D-F) Comparison of the preoviposition period, oviposition period and the fecundity of *C*Las+
123 and *C*Las- adults. Data are shown as means ± SEM. The significant differences between
124 *C*Las-positive and *C*Las-negative psyllids were determined using Student's *t*-tests (**$P < 0.01$,
125 ***$P < 0.001$).
126
127 ***DcAKH* is involved in changes in metabolism and fecundity in *D. citri* mediated by *C*Las**
128 Using our transcriptome database, cDNA sequences of *DcAKH* were identified and cloned.
129 The cDNA sequence of *DcAKH* is 225 bp in length, encodes a deduced polypeptide of 74
130 amino acid residues and has the conserved structural characteristics of a neuropeptide. The
131 conserved structure was "signal peptide + mature peptide + related peptide", and the mature
132 peptide sequence of *Dc*AKH is "QVNFSPNW" (Figure S1A). A phylogenetic analysis was
133 conducted to evaluate the association of *Dc*AKH with other insect AKHs; *Dc*AKH was most
134 closely related to the AKHs of three hemipteran species, *Nilaparvata lugens*, *Sitobion avenae*
135 and *Acyrthosiphon pisum* (Figure S1B).
136 Tissue expression profiles showed that *Dc*AKH was expressed at the highest level in the
137 brain, significantly higher than in the ovaries, fat bodies, and midgut in *D. citri* (Figure S2). The
138 levels of *DcAKH* in ovaries of *C*Las-negative and -positive psyllids decreased during the
139 assessment period. However, levels in the ovaries of *C*Las-positive psyllids were significantly
140 higher than those that were *C*Las-negative at all assessment times (Figure 2A). To investigate
141 the role of *DcAKH* in metabolic and reproductive changes induced by *C*Las, we knocked down
142 *DcAKH* expression using RNAi. When fed with ds*DcAKH*, the mRNA level of *DcAKH* in
143 *C*Las-negative and *C*Las-positive ovaries significantly decreased by 89% and 66%,
144 respectively, compared with psyllids fed with ds*GFP* (Figure 2B). Knockdown of *DcAKH*
145 resulted in TAG accumulation and a significant decrease in glycogen (Figures 2C-D).
146 Correspondingly, depletion of *DcAKH* led to a significant increase the size of the lipid droplets
147 (Figure 2E). Compared with the controls, *DcAKH* RNAi slowed ovarian development (Figure
148 2F), extended the preoviposition period (from 13.3 to 14.2 days in *C*Las-negative psyllids and

149 from 10.7 to 13.4 days in *C*Las-positive psyllids), shortened the oviposition period (from 7.1 to
150 4.3 days in *C*Las-negative psyllids and from 10.1 to 5.7 days in *C*Las-positive psyllids), and
151 decreased fecundity (from 138.0 to 94.7 days in *C*Las-negative psyllids and from 230.0 to
152 118.1 days in *C*Las-positive psyllids) (Figures 2G-I). Furthermore, the *C*Las signal and relative
153 titer in the ovaries of *DcAKH* knockdown psyllids significantly decreased (Figures 2J-K). Taken
154 together, it can be concluded that *DcAKH* is involved in *C*Las-induced metabolic and
155 reproductive changes in *D.citri.*

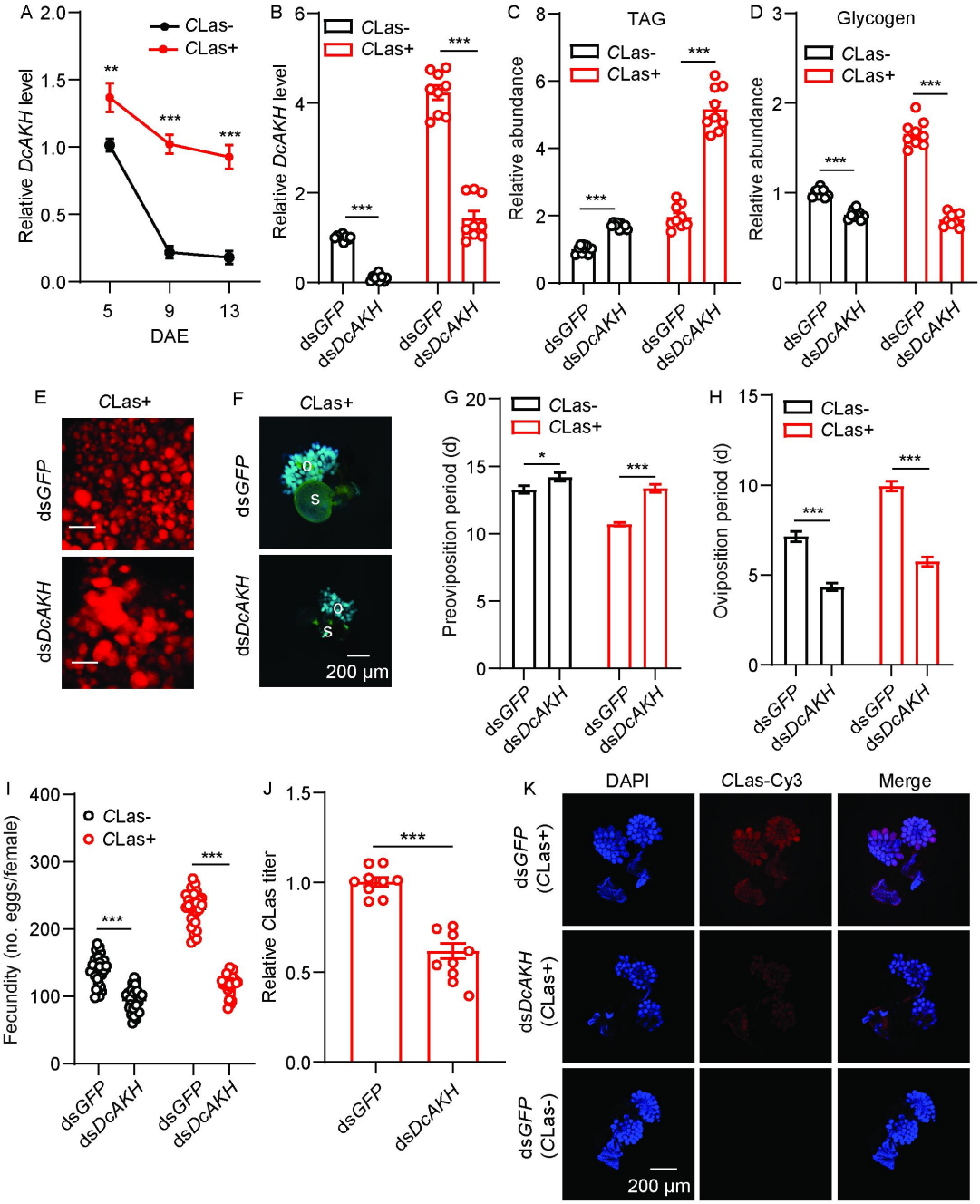

Figure 2. *DcAKH* is involved in the mutualistic relationship between *C*Las and *D. citri* resulting in increased fecundity. (A) Comparison of temporal expression patterns of *DcAKH* between the ovaries of *C*Las- and *C*Las+ psyllids. (B) Efficiency of RNAi of *DcAKH* in *C*Las- and *C*Las+ females treated with ds*DcAKH* for 48 h. (C) Comparison of TAG levels in fat bodies of *C*Las- and *C*Las+ females treated with ds*DcAKH* for 48 h. (D) Comparison of glycogen levels in fat bodies of *C*Las- and *C*Las+ females treated with ds*DcAKH* for 48 h. (E) Lipid droplets stained with Nile red in fat bodies dissected from *C*Las+ females treated with ds*DcAKH* for 48 h. Scale bar = 40 μm. (F) Ovary phenotypes of *C*Las+ females treated with

165 ds*DcAKH* for 48 h. Scale bar = 200 μm. o: ovary, s: spermathecae. (G-I) Comparison of the
166 preoviposition period, oviposition period and the fecundity between *C*Las- and *C*Las+ adults
167 treated with ds*DcAKH*. (J) The *C*Las titer in ovaries of *C*Las+ females treated with ds*DcAKH*
168 for 48 h. (K) Representative confocal images of *C*Las in the reproductive system of *C*Las+
169 females treated with ds*DcAKH* for 48 h. Scale bar = 200 μm. DAPI: the cell nuclei were stained
170 with DAPI and visualized in blue. *C*Las-Cy3: the *C*Las signal visualized in red by staining with
171 Cy3. Merge: merged imaging of co-localization of cell nuclei and *C*Las. Data are shown as
172 means ± SEM. The significant differences between treatment and controls are indicated by
173 asterisks (Student's *t*-test, $^{*}P < 0.05$, $^{**}P < 0.01$, $^{***}P < 0.001$).
174
175 ***DcAKHR* respond to *DcAKH* and participates in *D. citri*-CLas mutualism**
176 The protein tertiary structure of *DcAKHR* was predicted; *DcAKHR* has seven conserved
177 transmembrane (TM1-TM7) domains and is a typical G protein coupled receptor (Figure S3A).
178 A phylogenetic analysis was conducted to evaluate the association of *DcAKHR* with other
179 insect *AKHRs*; *DcAKHR* was most closely related to the *AKHR* of *Nilaparvata lugens* (Figure
180 S3B). To further confirm *Dc*AKH can activate *DcAKHR*, we performed a cell-based calcium
181 mobilization assay. As shown in Figure S3C, *DcAKHR* was strongly activated by *Dc*AKH in a
182 dose-dependent manner, with an EC_{50} value of 2.20×10^{-5} mM, but there were no responses
183 when challenged with an empty vector or other evolutionarily-related peptides. In addition,
184 after *DcAKH* knockdown, *DcAKHR* expression in the ovaries significantly decreased (Figure
185 S3D). *DcAKHR* was cloned, sequenced, designated and then used for further studies.
186 Sequence analysis showed that *DcAKHR* consisted of an open reading frame (ORF) of 1290
187 bp and a 185 bp 3' UTR. It encodes a putative protein consisting of 429 amino acids with a
188 predicted molecular weight of 48.32 kDa. Tissue expression patterns showed that *DcAKHR*
189 had the highest expression in the midgut, follow by the head, fat bodies, and ovaries (Figure
190 S4). In the ovaries of *C*Las-positive and -negative psyllids, the transcript and protein levels of
191 *DcAKHR* increased over the assessment period with levels of both being higher in
192 *C*Las-positive psyllids than in *C*Las-negative psyllids (Figure 3A). To investigate the role of
193 *DcAKHR* in metabolic and reproductive changes induced by *C*Las, we knocked down
194 *DcAKHR* expression by RNAi. When fed with ds*DcAKHR*, the mRNA levels of *DcAKHR* in the

195 ovaries of *C*Las-negative and *C*Las-positive were significantly decreased by 59.4 and 66.0%,
196 respectively, compared with psyllids fed with ds*GFP*; western blot analysis confirmed that
197 *Dc*AKHR protein levels were also significantly reduced (Figure 3B). Knockdown of *DcAKHR*
198 resulted in TAG accumulation and a significant decrease in glycogen (Figures 3C-D).
199 Correspondingly, depletion of *DcAKHR* led to a significant increase in the size of lipid droplets
200 (Figure 3E). Compared with the controls, *DcAKHR* RNAi interfered with ovarian development
201 (Figure 3F): the preoviposition period was extended (from 13.3 to 16.2 days in *C*Las-negative
202 psyllids and from 10.7 to 12.9 days in *C*Las-positive psyllids); oviposition period was shortened
203 (from 7.1 to 4.6 days in *C*Las-negative psyllids and from 10.1 to 5.3 days in *C*Las-positive
204 psyllids); and fecundity decreased (from 138.0 to 90.6 eggs per female in *C*Las-negative
205 psyllids and from 230.0 to 98.2 eggs per female in *C*Las-positive psyllids). These effects are
206 similar to those caused by *DcAKH* knockdown (Figures 3G-I). Furthermore, the *C*Las signal
207 and relative titer in the ovaries of *DcAKH* knockdown psyllids were significantly decreased
208 (Figures 3J-K). Taken together, *DcAKHR* responds to *DcAKH* and is involved in the
209 *C*Las-induced metabolic and reproductive changes in *D. citri.*
210

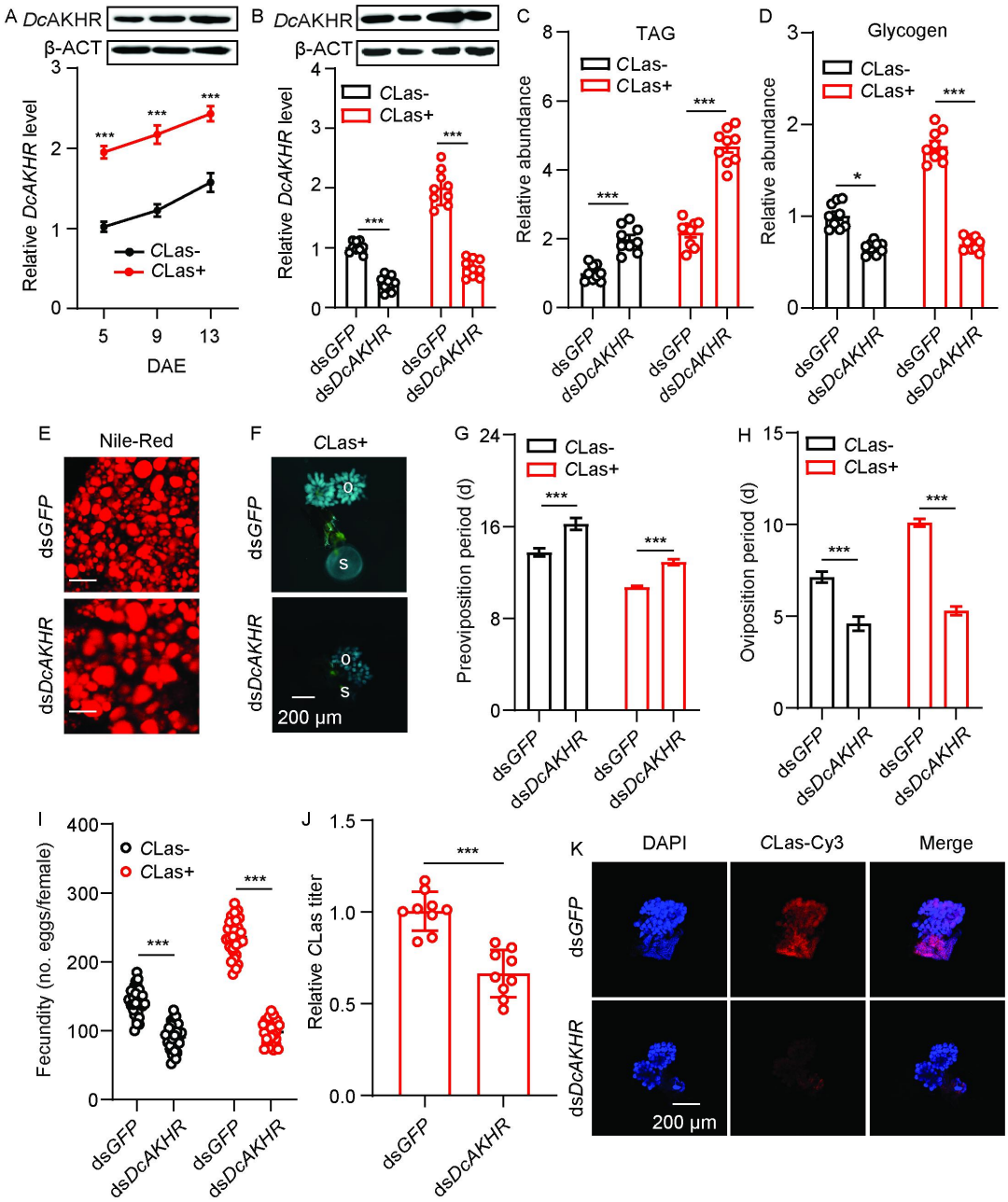

Figure 3. *DcAKHR* is involved in the mutualistic relationship between *C*Las and *D. citri* resulting in increased fecundity. (A) Comparison of temporal expression patterns of *DcAKHR* between the ovaries of *C*Las- and *C*Las+ psyllids. (B) The efficiency of RNAi of *DcAKHR* in *C*Las- and *C*Las+ psyllids treated with ds*DcAKHR* for 48 h. (C) Comparison of TAG levels in fat bodies of *C*Las- and *C*Las+ females treated with ds*DcAKHR* for 48 h. (D) Comparison of glycogen levels in fat bodies of *C*Las- and *C*Las+ females treated with ds*DcAKHR* for 48 h. (E) Lipid droplets stained with Nile red in fat bodies dissected from *C*Las-positive females treated with ds*DcAKHR* for 48 h. Scale bar = 40 μm. (F) Ovary

220 phenotypes of *C*Las+ females treated with ds*DcAKHR* for 48 h. Scale bar = 200 μm. o: ovary,
221 s: spermathecae. (G-I) Comparison of the preoviposition period, oviposition period and the
222 fecundity of *C*Las- and *C*Las+ adults treated with ds*DcAKHR*. (J) The *C*Las titer in the ovaries
223 of *C*Las+ females treated with ds*DcAKHR* for 48 h. (K) Representative confocal images of the
224 reproductive system of *C*Las+ females treated with ds*DcAKHR* for 48 h. Scale bar = 200 μm.
225 DAPI: the cell nuclei were stained with DAPI and visualized in blue. *C*Las-Cy3: the *C*Las signal
226 visualized in red by staining with Cy3. Merge: merged imaging of co-localization of cell nuclei
227 and *C*Las. Data are shown as means ± SEM. The significant differences between treatment
228 and controls are indicated by asterisks (Student's *t*-test, ***$P < 0.001$).
229
230 **miR-34 targeted *DcAKHR***
231 Based on the small RNA libraries of *D. citri*, we used miRanda and RNAhybrid software to
232 predict the potential miRNAs targeting *DcAKHR*; three putative miRNAs, namely miR-34,
233 miR-2 and miR-14 (Figure 4A), were identified. To confirm the binding activity of these miRNAs
234 with *DcAKHR*, several dual-luciferase reporter assays were conducted. Compared with the
235 controls, the luciferase activity was markedly reduced when miR-34 agomir was co-transfected
236 with the recombinant plasmid containing the full 3'UTR sequence of *DcAKHR*, while miR-2 and
237 miR-14 activities were not significantly changed (Figure 4B). In addition, the reporter activity
238 was recovered when the binding sites of miR-34 were mutated in the *DcAKHR* 3'-UTR (Figure
239 4C). To determine whether miR-34 specifically targets *DcAKHR*, the following experiments
240 were conducted. Firstly. tissue expression patterns showed that the miR-34 was highly
241 expressed in the head, followed by the fat bodies, ovaries, and midgut (Figure 4D). Secondly,
242 miR-34 has the opposite expression pattern to *DcAKHR* (Fig. 3A), and transcript levels
243 decreased over the assessment period with the levels of both being lower in *C*Las-positive
244 psyllids than in *C*Las-negative psyllids (Figure 4E). Thirdly, after feeding with agomir-34, the
245 relative levels of miR-34 mRNA in the ovaries of *C*Las-negative and *C*Las-positive psyllids
246 increased 1.9- and 2.3-fold, respectively (Figure S5). The mRNA and protein levels of
247 *DcAKHR* were correspondingly increased or decreased after separately feeding psyllids with
248 either antagomir-34 or agomir-34 (Figure 4F). Fourthly, an RNA immunoprecipitation (RIP)
249 assay was performed; *DcAKHR* mRNA was significantly enriched in the

250 anti-AGO-immunoprecipitated RNAs from ovaries of agomir-34-fed female psyllids relative to
251 the control samples (Figure 4G). Taken together, these results strongly suggest that *DcAKHR*
252 is a direct target of miR-34.

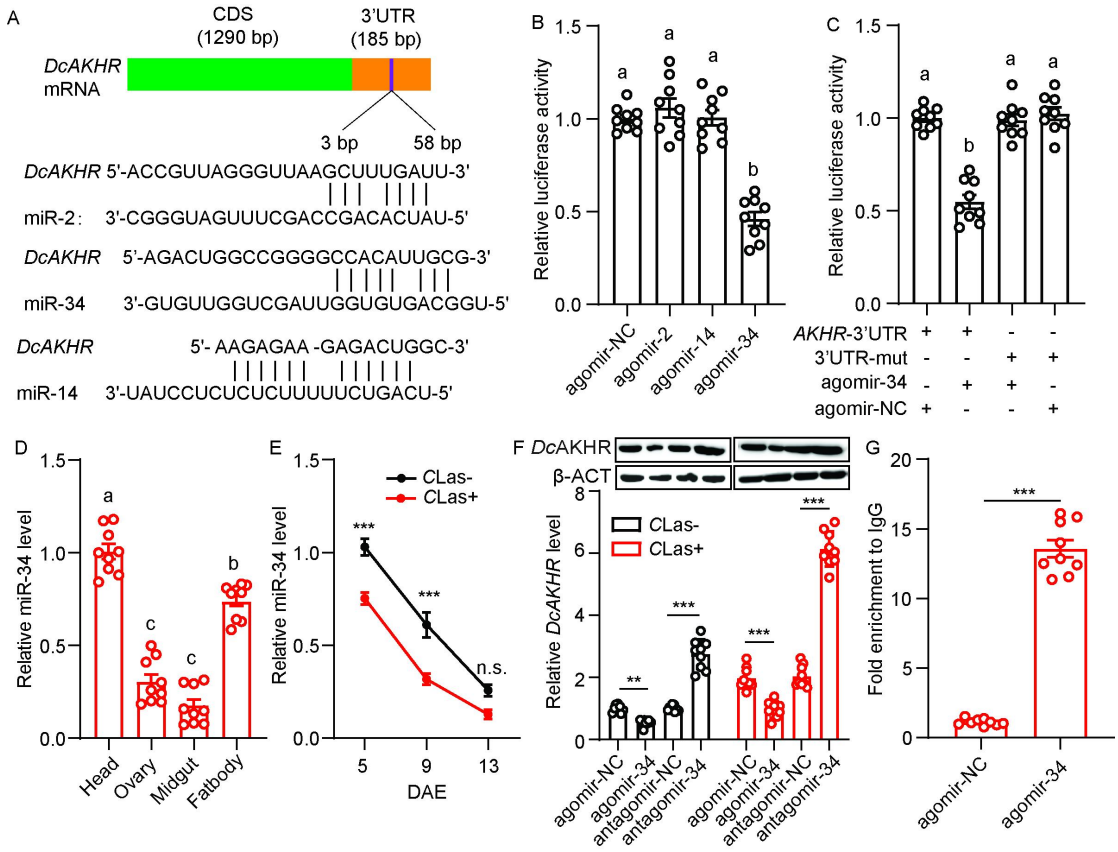

253

254 **Figure 4. Identification and validation of the target relationship between miR-34 and**
255 ***DcAKHR.*** (A) The putative binding sites of miRNAs in the *DcAKHR* 3'-UTR as predicted by
256 miRanda and RNAhybrid. (B) Dual-luciferase reporter assays using HEK293T cells
257 co-transfected with miRNA agomir and recombinant pmirGLO vectors containing the predicted
258 binding sites for miR-2, miR-14 and miR-34 in the CDS of *DcAKHR.* (C) Dual-luciferase
259 reporter assays using HEK293T cells co-transfected with miR-34 agomir plus recombinant
260 pmirGLO vectors containing *DcAKHR*-3'UTR or mutated *DcAKHR*-3'UTR. (D) Tissue
261 expression pattern of miR-34 in *C*Las+ female adults at 7 DAE in the head, ovary, fat body,
262 and midgut. (E) Comparison of temporal expression patterns of miR-34 in ovaries of *C*Las-
263 and *C*Las+ females. (F) Effect of miR-34 agomir and antagomir treatments on *Dc*AKHR mRNA
264 expression and protein level in ovaries of *C*Las- and *C*Las+ psyllids after 48 h. (G) Relative
265 expression of miR-34 targeted *DcAKHR in vivo* as demonstrated by an RNA
266 immunoprecipitation assay. Data are shown as mean ± SEM. For B-D, significant differences

267 among the different treatments are indicated by lowercase letters above the bars (one-way
268 ANOVA followed by Tukey's Honestly Significant Difference test at $P < 0.05$). The significant
269 differences between treatment and control are indicated by asterisks in E-G (Student's *t*-test,
270 $^{**}P < 0.01$, $^{***}P < 0.001$).
271

272 **miR34 participates in *D. citri*-*C*Las mutualism in ovaries**

273 To investigate the roles of miR-34 in the interaction between *D. citri* and *C*Las,
274 *C*Las-positive and –negative females were fed with agomir-negative control (NC) or with
275 miR-34 agomir. After feeding with miR-34 agomir, there was a significant accumulation of TAG
276 and a decrease in glycogen levels in the two populations (Figures 5A-B). The size of lipid
277 droplets in the fat bodies of *C*Las-positive psyllids were bigger than those of the control (Figure
278 5C). After treatment with miR-34 agomir, ovarian development of *C*Las-positive psyllids was
279 reduced (Figure 5D). In addition, when *C*Las-negative and *C*Las-positive psyllids were fed with
280 miR-34 agomir, the oviposition period of both psyllid types was shortened, preoviposition
281 period was markedly extended, and fecundity significantly decreased compared with the
282 relevant control groups (Figures 5E-G); these phenotypes mimic those expressed after
283 treatment with ds*DcAKHR*. Moreover, the *C*Las signals and relative titer in *C*Las-positive
284 ovaries were significantly reduced (Figures 5H-I). All the results indicate that miR-34
285 suppresses *DcAKHR* expression and is involved in the mutualistic interaction.

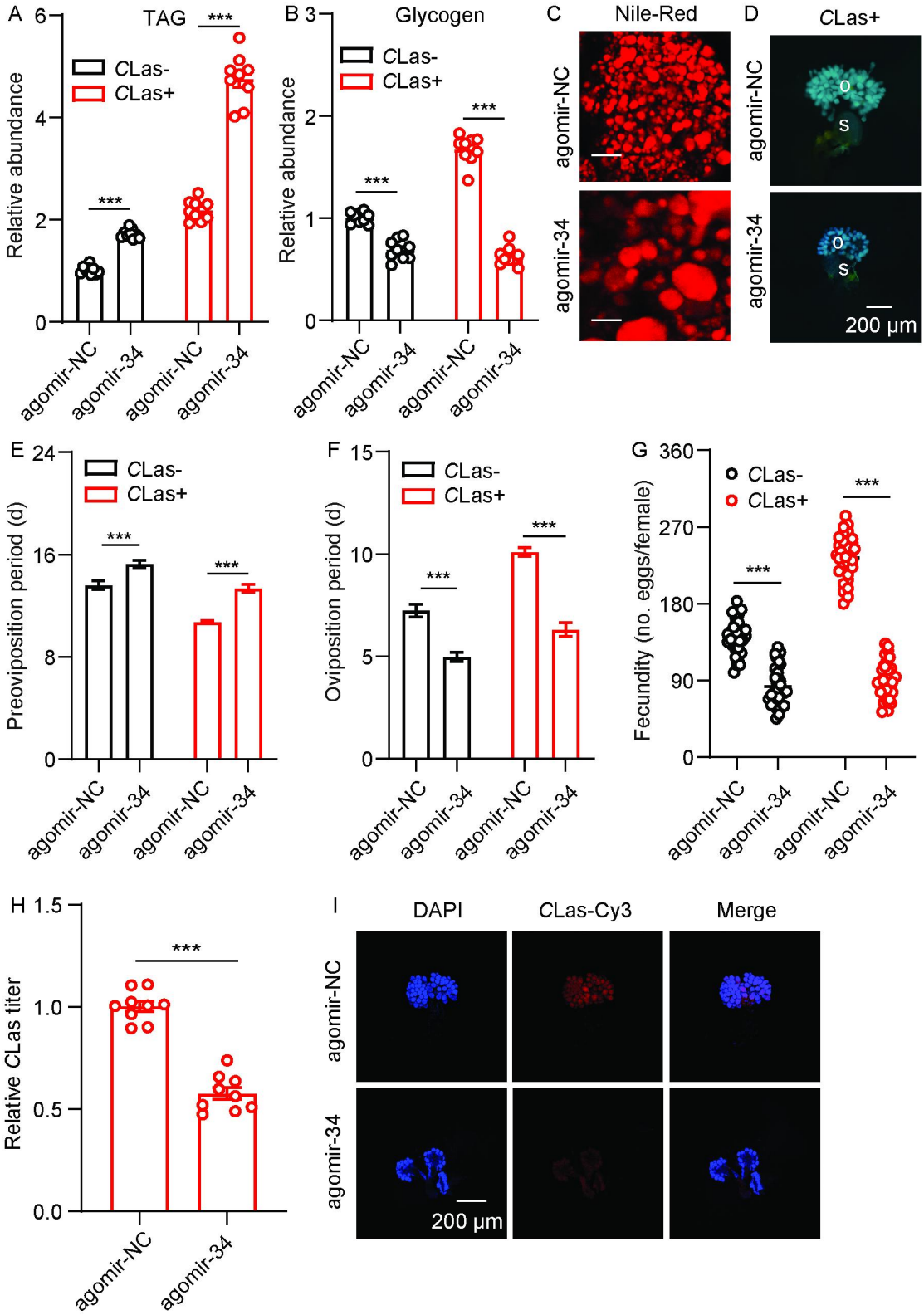

Figure 5. miR-34 participation in mutualistic interactions between *D. citri* and *C*Las. (A) Comparison of TAG levels in fat bodies of *C*Las- and *C*Las+ females treated with agomir-34 for 48 h. (B) Comparison of glycogen levels in the fat bodies of *C*Las- and *C*Las+ females treated with agomir-34 for 48 h. (C) Lipid droplets stained with Nile red in fat bodies

291 dissected from *C*Las+ females treated with agomir-34 for 48 h. Scale bar = 40 μm. (D) Ovary
292 phenotypes of *C*Las+ female treated with agomir-34 for 48 h. Scale bar = 200 μm. o: ovary, s:
293 spermathecae. (E-G) Comparison of the preoviposition period, oviposition period and the
294 fecundity between *C*Las- and *C*Las+ adults treated with agomir-34. (H) *C*Las titer in ovaries of
295 *C*Las+ females treated with agomir-34 for 48 h. (I) Representative confocal images of *C*Las in
296 the reproductive system of *C*Las+ females treated with agomir-34 for 48 h. Scale bar = 200 μm.
297 The signals of DAPI and *C*Las-Cy3 are same as described in Figure 2. Data are shown as
298 means ± SEM. The significant differences between treatment and controls are indicated by
299 asterisks (Student's *t*-test, ***$P < 0.001$).
300
301 **The JH signaling pathway is regulated by the AKH pathway and is involved in the**
302 **increase in fecundity induced by *C*Las**
303 To evaluate whether the JH signaling pathway is regulated by the AKH signaling pathway,
304 we assayed the relative JH titers and the expression levels of several JH pathway-related
305 genes in *DcAKH*-deficient, *C*Las-positive females. Compared to control females, the relative
306 JH titer in the abdomen decreased significantly after *dsDcAKH* treatment for 48 h (Figure 6A).
307 After feeding with *dsDcAKH* for 48 h, the expression levels of the JH receptor gene, *DcMet,*
308 and the downstream transcription factor, *DcKr-h1*, of the JH signaling pathway were
309 significantly reduced in the fat bodies and ovaries (Figures 6B-C). In addition, the expression
310 levels of *DcVg1-like*, *DcVgA1-like* and *DcV*gR, three important downstream genes of the JH
311 signaling pathway related to ovarian development were lower in *DcAKH*-deficient
312 *C*Las-positive females than in controls after dsRNA feeding for 48 h (Figures 6B-C). Similar
313 results were observed in the *DcAKHR*-deficient *C*Las-positive females (Figures 6D-F) as well
314 as *C*Las-positive females fed with agomir-34 (Figures 6G-I). These results suggest that JH
315 signaling pathway is regulated by the AKH-AKHR-miR-34 signaling pathway and is involved in
316 the increased fecundity of *D. citri* induced by *C*Las.

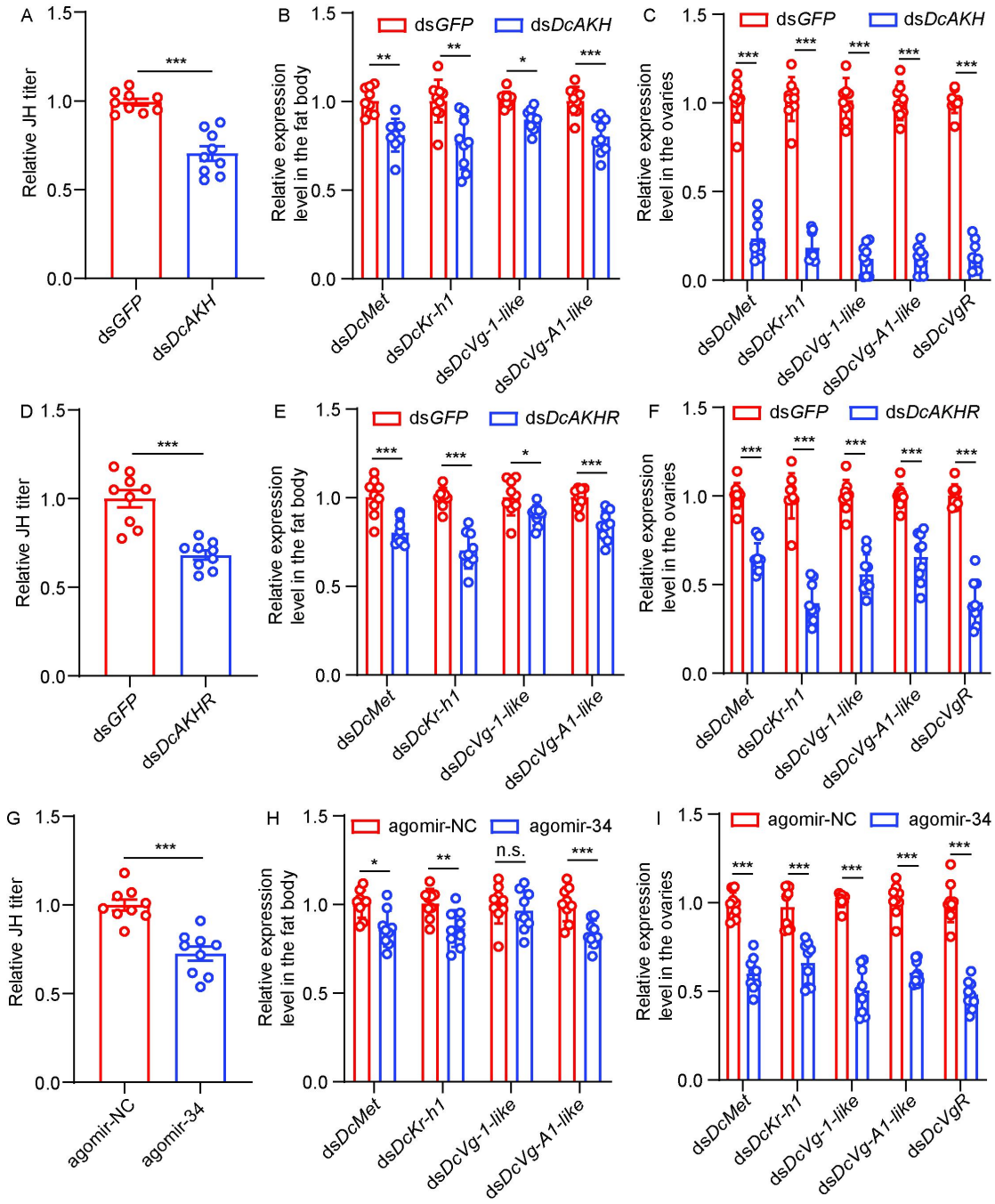

317

318 **Figure 6. The JH signaling pathway is regulated by AKH signaling pathway and is**
319 **involved in the increase in fecundity of *D. citri* induced by *C*Las.** (A) JH titer in the
320 abdomen of *C*Las+ females treated with ds*DcAKH* for 48 h. (B) Effects of ds*DcAKH* treatment
321 on mRNA level of JH signaling pathway in fat bodies of *C*Las+ females. (C) Effects of
322 ds*DcAKH* treatment on mRNA levels of components of the JH signaling pathway in the ovaries
323 of *C*Las+ females. (D) JH titers in the abdomens of *C*las+ females treated with ds*DcAKHR* for
324 48 h. (E) Effects of ds*DcAKHR* treatment on mRNA level of JH signaling pathway in fat bodies
325 of *C*Las+ females. (F) Effects of ds*DcAKHR* treatment on mRNA levels of components of the

326 JH signaling pathway in ovaries of *C*Las+ females. (G) JH titer in abdomen of *C*Las+ females
327 treated with agomir-34 for 48 h. (H) Effects of agomir-34 treatment on mRNA levels of
328 components of the JH signaling pathway in fat bodies of *C*Las+ females. (I) Effects of
329 agomir-34 treatment on mRNA levels of components of the JH signaling pathway in the
330 ovaries of *C*Las+ females.
331

332 ## Discussion

333 Increasing numbers of studies have focused on the effects of vector-virus interactions on
334 reproduction. For example, rice gall dwarf virus is vertically transmitted by hitchhiking on insect
335 sperm, thereby promoting long-term viral epidemics and persistence in nature [2]. Berasategui
336 et al. (2022) [3] found a mutualistic relationship between *Chelymorpha alternans* and *Fusarium*
337 *oxysporum*, where the pupae were protected in exchange for the dissemination and
338 propagation of the fungus. There are few studies on the mechanisms underlying
339 vector-bacteria interactions. However, Singh and Linksvayer (2020) [38] found that
340 *Wolbachia*-infected colonies of *Monomorium pharaonis* had increased colony-level growth,
341 accelerated colony reproduction, and shortened colony life cycles compared to those that were
342 uninfected.

343 The fat body is the major insect storage organ that produces the majority of
344 hemolymph-born vitellogenic proteins and critically contributes to insect ovary development
345 [16]. In this study, after infection with *C*Las, the preoviposition period of *D. citri* was shortened,
346 oviposition period was prolonged, and fecundity was significantly increased. These results
347 suggests that there is a mutualistic interaction in *D. citri* ovaries with *C*Las. *C*Las accelerates
348 ovarian development and prolongs the oviposition period thereby enhancing the fecundity of *D.*
349 *citri*; in turn, *D. citri* provides sites and nutrients for *C*Las replication during ovarian
350 development. *C*Las-positive *D. citri* require more energy to support this increased fecundity.
351 Hence, the TAG and glycogen levels of both *C*Las-positive and *C*Las-negative were assayed.
352 After infection with *C*Las, the TAG and glycogen levels significantly increased, and the average
353 size of lipid droplets in the fat bodies were distinctly larger, indicating that the increase in lipid
354 mobilization may prepare for an increase in fecundity.

355 The total amount of lipids present in fat bodies is a balance between lipogenesis and

356 lipolysis [39], and both processes are essential for lipid homeostasis. Disruption of either
357 lipogenesis or lipolysis could interfere with nutritional and physiological conditions in fat bodies
358 and affect vitellogenesis. AKH/AKHR mediated lipolytic systems are essential for lipid
359 provision and nutrient transfer during reproduction. In *Gryllus bimaculatus* [40,41] and
360 *Caenorhabditis elegans* [42], injections of AKH interfered with egg production by inhibiting the
361 production of vitellogenins and the accumulation of lipid stores. In *Bactrocera dorsalis*, AKHR
362 knockdown led to decreased lipolytic activity and delayed oocyte maturation [27] and these
363 authors suggested the decline in fecundity may be due to the inability to utilize the lipid stores
364 of fat bodies to promote oocyte maturation. In *Glossina morsitans*, the silencing of *AKHR* and
365 *brummer* led to the inability to mobilize lipid reserves in fat bodies during pregnancy, slowed
366 down the development of oocytes, and caused embryogenesis to fail, indicating that female
367 fertility depends on lipid metabolism regulated by AKHR [24]. These results suggest that lipid
368 homeostasis appears critical for insect fecundity, as its disruption substantially suppresses egg
369 production and negatively affects vitellogenesis.

370 In the present study, *DcAKH* and *DcAKHR* played important roles in the increased lipid
371 metabolism and fecundity of *D. citri* mediated by *C*Las. The cDNA sequences encoding AKH
372 and AKHR from *D. citri* were cloned and identified, and phylogenetic analysis showed that
373 *DcAKH* and *DcAKHR* were orthologous to other hemipteran AKHs and AKHRs. Functional
374 analysis showed that *DcAKHR* shares properties found with other AKHRs.
375 *DcAKHR*-transfected CHO cells could be activated by AKH peptide, while it did not response
376 to Crz peptide, despite the sequences and gene structures of AKH and Crz being closely
377 related [21]. *DcAKH* and *DcAKHR* were more highly expressed in the ovaries of *C*Las-positive
378 psyllids than those of *C*Las-negative individuals. Knockdown of *DcAKH* and *DcAKHR* resulted
379 in TAG accumulation and a significant decrease in glycogen levels in the fat bodies. Most
380 importantly, the *C*Las titer in the ovaries of *C*Las-positive psyllids and fecundity significantly
381 reduced when feeding with *dsDcAKH* and *dsDcAKHR*. Our results support the idea that
382 reproductive disruption from AKH/AKHR knockdown is due to the inability of female to mobilize
383 lipid reserves in the fat bodies required for oocyte maturation during vitellogenesis.

384 To date, there are no reports on the post-transcriptional regulation of AKHR. As important
385 post-transcriptional regulators, miRNAs generally suppress their target genes by triggering

386 mRNA degradation or translational repression [30]. More and more miRNAs have been
387 reported to be involved in the metabolic processes of insects including reproduction. In
388 addition to functions of miR-277 described in the Introduction, this miRNA targets ilp7 and ilp8
389 thereby controlling lipid metabolism and reproduction in *A. aegypti* [37]. miR-8 depletion in
390 mosquitoes resulted in an increase of its target gene, *secreted wingless-interacting molecule*,
391 and in lipid accumulation in developing oocytes [43]. Depletion of miR-8 in mosquitoes by
392 antagomir injection upregulates *secreted wingless-interacting molecule* and decreases the
393 level of lipid in ovaries to block vitellogenesis post blood meals [44]. A switch from catabolic to
394 anabolic amino acid metabolism in fat bodies mediated by miR-276 restricts mosquito
395 investment into oogenesis and benefits the development of *Plasmodium falciparum* [45]. In the
396 current study, based on *in vitro* and *in vivo* experiments, we found that host miR-34 targets
397 *DcAKHR*. miR-34 was observed to have an opposite expression trend to *DcAKHR*, and its
398 expression in the ovaries of *C*Las-positive psyllids was lower than in those of CLas-negative
399 individuals. Treatment of miR-34 agomir and antagomir, respectively, resulted in a significant
400 decrease and increase in *DcAKHR* mRNA and protein levels. In addition, miR-34
401 overexpression not only led to the accumulation of TAG and the reduction of glycogen levels in
402 fat bodies, but also decreased fecundity and *C*Las titers in the ovaries similar to the
403 phenotypes caused by silencing of *DcAKHR*. This indicates that *C*Las inhibited host miR-34 to
404 enhance *DcAKHR* expression and improve the lipid metabolism and fecundity. This study is
405 the first to report the manipulation of host miRNAs and target genes by a bacterium to affect
406 lipid metabolism and reproduction of their vector.

407 Vitellogenesis is strongly linked with insect JH production [46]. The fat body is an
408 important tissue that senses and integrates various nutritional and hormonal signals required
409 for the regulation of vitellogenesis [16]. Moreover, JH is also involved in the nutrient-dependent
410 regulation of insect reproduction, but the mechanism of action remains obscure. Lu et al.
411 (2016a, b) [47,48] have demonstrated that nutritional signaling during female reproduction
412 induces JH biosynthesis that in turn stimulates vitellogenin expression in fat bodies and egg
413 production in *N. lugens.* In order to evaluate the possible relationship between
414 AKH/AKHR-mediated lipolysis and JH-dependent vitellogenesis, the expressions of JH
415 signaling pathway-related genes in fat bodies and ovaries were determined after knockdown of

416 *DcAKH* and *DcAKHR*. We found that reducing *DcAKH* or *DcAKHR* by RNAi in *C*Las-positive *D.*
417 *citri* not only decreased JH titer but also resulted in a decrease in the expression of *DcMet* and
418 *DcKr-h1* in the fat bodies and ovaries, as well as the egg development related genes,
419 *DcVg-1-like*, *DcVg-A1-like* and *DcVgR*. Similar results were detected in the agomir-34
420 treatment. Our results suggest that AKH/AKHR-based lipolysis plays an important regulatory
421 role in the JH signaling pathway during *D. citri*-*C*Las interactions.

422 In conclusion, we proposed the scheme of events following *C*Las infection presented in
423 Figure 7. After infection with *C*Las, *D. citri* are more fecund than their uninfected counterparts.
424 The interaction between *C*Las and *D. citri* affecting reproduction is a win-win strategy; the
425 more offspring of *D. citri*, the more *C*Las in the field. *C*Las upregulates the AKH/AKHR
426 signaling and downregulates miR-34 to increase lipid metabolism and activate JH-dependent
427 vitellogenesis, thereby improving the fecundity of *C*Las-positive females. Overall, our results
428 not only broaden our understanding of the molecular mechanism underlying the *D. citri*-*C*Las
429 interaction, but also provide valuable information for further integrated management of *D.citri*
430 and HLB by targeting the *DcAKH/DcAKHR* signaling pathway.
431

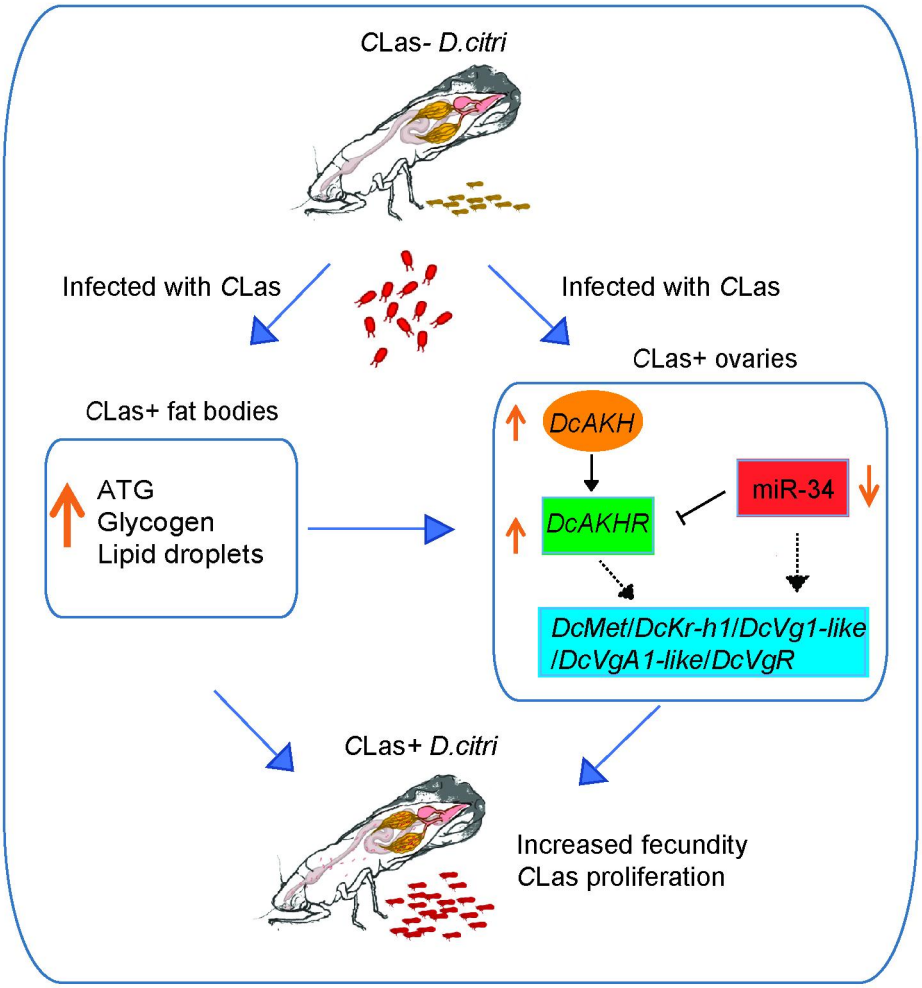

Figure 7. Mechanisms linking metabolism and reproduction of *D. citri* induced by CLas. After infection with CLas, the TAG and glycogen levels in fat bodies of CLas-positive psyllids significantly increased as well as the size of lipid droplets. In ovaries, CLas upregulates the AKH/AKHR signaling and downregulates miR-34 to increase lipid metabolism and activate JH-dependent vitellogenesis, thereby improving the fecundity of CLas-positive females. *D. citri* are more fecund than their uninfected counterparts. The interaction between CLas and *D. citri* affecting reproduction is a win-win strategy; the more offspring of *D. citri*, the more CLas in the field.

442 ## Materials and Methods

443 **Host plants and insect colonies**

444 The *C*Las-negative (healthy) and *C*Las-positive *D. citri* colonies were obtained from a
445 laboratory culture continuously reared on the healthy and *C*Las-infected lemon (*Citrus ×limon*
446 (L.) Osbeck) plants. The *C*Las-infected lemon plants and psyllids were monitored to detect
447 *C*Las infection monthly using the quantitative polymerase chain reaction (qPCR). The two
448 populations were raised in different incubators with same conditions (26 ± 1 ℃, 65 ± 5%
449 relative humidity (RH) and a 14-h light: 10-h dark cycle). *C*Las-negative and *C*Las-positive
450 lemon plants were grown in two separate glasshouses.

451

452 **Bioinformatics and phylogenetic analyses**

453 The physicochemical properties of *DcAKH* (GenBank accession number: MG550150.1)
454 and *DcAKHR* (GenBank accession number: OR259432) were analyzed using the online
455 bioinformatics ProtParam tool (http://web.expasy.org/protparam/). Homologous protein
456 sequences of AKH and AKHR were aligned with those of other insects using DNAman6.0.3
457 software. Phylogenetic trees were constructed with the neighbor-joining method in MEGA5.10
458 software, with 1000 bootstrap replicates; bootstrap values > 50% shown on the tree.

459

460 **Assays of reproductive parameters**

461 Tested females from two colonies were selected and paired with healthy males. One
462 female and one male were placed onto young vegetative shoots (flush) of healthy lemon plants
463 to promote oviposition; the flush and insects were sealed with tied white mesh bag (15 × 20
464 cm). These lemon plants were held in an incubator (25 ± 1 ℃, 65 ± 5% RH, 14L: 10D
465 photoperiod). After 24h, the preoviposition period and oviposition period were recorded, the
466 number of eggs laid per female were counted, and this pair of psyllids were transferred to new
467 flush to continue egg laying. Eggs were counted daily until all females died. All the experiments
468 were performed using three replications, and about 15 pairs of *D. citri* for each replication.

469

470 **Quantitative RT-PCR (qRT-PCR)**

471 For mRNA expression analysis, total RNA was extracted using TRIzol reagent (Invitrogen,

472 Carlsbad, CA, United States), and the synthesis of first-strand cDNA was performed using a
473 PrimeScript™ II 1st Strand cDNA Synthesis Kit (Takara, Beijing, China) in accordance with the
474 manufacturer's instructions. qRT-PCR was carried out by using the TB Green® Premix Ex
475 Taq™ II (Takara, Beijing, China) on an ABI PRISM® 7500 Real-Time System (Applied
476 Biosystems, Foster City, CA, USA). The beta-actin (Dcβ-ACT, GenBank XM_026823249.1)
477 gene was used as an internal control to normalize gene expression levels. For miRNA
478 expression analysis, miRNA was extracted using a miRcute miRNA Isolation Kit (TIANGEN,
479 Beijing, China), synthesized using a miRcute Plus miRNA First-Strand cDNA Kit (TIANGEN,
480 Beijing, China), and quantified using the miRcute Plus miRNA qPCR Kit (SYBR Green)
481 (TIANGEN, Beijing, China). U6 snRNA was used as an internal control to normalize the
482 expression of miRNA. All the primers used are listed in Supplementary Table 1.
483
484 **Luciferase activity assay**
485 The 185 bp sequence of the 3'UTR containing the predicted target sites for miR-34 in
486 *DcAKHR* was cloned into the pmirGLO vector (Promega, Wisconsin, USA) downstream of the
487 luciferase gene to construct the recombinant plasmid, *DcAKHR*-3'UTR-pmirGLO, using the
488 pEASY®-Basic Seamless Cloning and Assembly Kit. The mutated 3'UTR sequence was
489 amplified and cloned into the pmirGLO vector to generate the *DcAKHR*-3'UTR
490 mutant-pmirGLO plasmid. The agomir and antagomir of miRNAs were chemically synthesized
491 and modified by GenePharma (Shanghai, China) with chemically modified RNA oligos of the
492 same sequence or anti-sense oligonucleotides of the miRNA. The negative control for agomir
493 and antagomir was provided by the manufacturer. According to the manufacturer's instructions,
494 the constructed vector (500 ng) and miRNA agomir (275 nM) were co-transferred into
495 HEK293T cells in a 24-well plate using a Calcium Phosphate Cell Transfection Kit (Beyotime,
496 Nanjing, China). After co-transfection for 24 h, the activities of firefly and Renilla luciferase
497 were detected using the Dual-Glo Luciferase Assay System (Promega, Madison, WI, USA),
498 and the average luciferase activity was calculated.
499

500 **Fluorescence in situ hybridization (FISH)**

501 FISH using a *C*Las probe was carried out as previously described [49]. Under a dissecting
502 microscope, the ovaries of *C*Las-negative and *C*Las-postive *D. citri* were dissected in 1 ×
503 phosphate-buffered saline (PBS) (Beyotime Biotechnology, Shanghai, China). Firstly, the
504 isolated ovaries were fixed in Carnoy's fixative (glacial acetic acid-ethanol-chloroform, 1: 3: 6,
505 vol/vol) for 12 h at 25 ℃, washed four times (5 min each time) with 6% H_2O_2 in 80% ethanol
506 and then three times (10-15 min per time) with PBST (1 × PBS: TritonX-100, 99.7: 0.3,
507 (vol/vol)). Secondly, the samples were pre-incubated three times (10 min per time) in
508 hybridization buffer (20 mM Tris-HCl, pH 8.0, 0.9 M NaCl, 30% formamide (vol/vol), 0.01%
509 sodium dodecyl sulfate (wt/wol)) containing 10 pmol/mL of each probe for 24 h at 25 ℃, then
510 washed three times with PBST. Thirdly, nuclei were stained with 0.1 mg/mL of 40,
511 60-diamidino-2-phenylindole (DAPI) (Sigma-Aldrich, St Louis, MO, USA) for 15 min, then
512 washed once with PBST. Finally, the stained ovaries were mounted in mounting medium. The
513 slides were scanned under a Leica TCS-SP8 (Leica Microsystems Exton, PA USA) confocal
514 microscope; excitation lasers emitting at 405 nm and 550 nm were used to detect the DAPI
515 and Cy3 signals, respectively, and sequential scanning was used to avoid the signal overlap of
516 probes. Image processing was completed using Leica LAS-AF software (v2.6.0). Specificity of
517 detection was carried out using without the probe and *C*Las-negative controls. Three FISH
518 tests were performed and at least 20 ovaries were viewed under the microscope to confirm the
519 repeatability. The probe sequences used in the current study are listed in Supplementary Table
520 1.

521

522 **Western blotting**

523 The total proteins from *D. citri* ovaries were extracted using RIPA protein lysis buffer (50
524 mM Tris pH 7.4, 1% Triton X-100, 150 mM NaCl, 1% sodium deoxycholate and 0.1% SDS)
525 with 1 mM PMSF. Proteins concentrations were quantified using a BCA protein assay kit
526 (Beyotime, Jiangsu, China). Aliquots of 60 μg protein were separated by 12% SDS-PAGE and
527 transferred to polyvinylidene fluoride membranes (Millipore). Subsequently, the membranes
528 were incubated with the primary antibody against *DcAKHR* (1: 1000 dilution, ABclonal
529 Technology Co., Ltd., Wuhan, China) for 12 h at 4 °C and then with the secondary antibody

530 (goat anti-rabbit IgG conjugated with HRP, 1: 10000 dilution) for 2 h at 25 °C. A mouse
531 monoclonal antibody against β-actin (TransGen Biotech, Beijing, China) was used as a control.
532 Immunoreactivity was imaged with the enhanced chemiluminescence with Azure C600
533 multifunctional molecular imaging system.
534
535 **Nile red staining**
536 The fat bodies were dissected from adult females 5 DAE, fixed in 4% paraformaldehyde
537 for 30 min at 25 ℃, and washed twice with 1 × PBS. Lipid droplets were incubated for 30 min
538 within the mixture of Nile red (0.1 μg/μL) and DAPI (0.05 μg/μL), and then washed twice with 1
539 × PBS. The samples were imaged using a laser scanning microscopy (TCS-SP8, Leica
540 Microsystems Exton, PA USA).
541
542 **Determination of TAG levels**
543 TAG levels were measured using a Triglycerides Colorimetric Assay (Cayman) in
544 accordance with the manufacturer's instructions. In short, thirty fat bodies were homogenized
545 in 100 μL of Diluent Assay Reagent. Then 10 μL of supernatant was incubated with Enzyme
546 Mixture solution, the TAG contents from the measurements were normalized to protein levels
547 in the supernatant of the samples determined using a BCA protein assay (Thermo Fisher
548 Scientific). Three independent biological replicates were analyzed for each treatment, and
549 each treatment included three technical replicates.
550
551 **Determination of glycogen levels**
552 Glycogen levels were assayed using a Glycogen Assay Kit (Cayman) in accordance with
553 the manufacturer's instructions. In brief, thirty fat bodies were homogenized in 100 μL of
554 Diluent Assay Reagent, and 10 μL of supernatant was incubated with Enzyme Mixture solution
555 and Developer Mixture. The glycogen levels from the measurements were normalized to
556 protein levels in the supernatant of the sample determined using a BCA protein assay (Thermo
557 Fisher Scientific). Three independent biological replicates were analyzed for each treatment,
558 and each treatment included three technical replicates.
559

560 **dsRNA synthesis and RNAi assay**

561 dsRNAs of *DcAKH* and *DcAKHR* were transcribed by a Transcript Aid T7 High Yield kit
562 (Thermo Scientific, Wilmington, DE, United states) and purified using the GeneJET RNA
563 Purification kit (Thermo Scientific). miRNA agomir, agomir negative control, miRNA antagomir,
564 and antagomir negative control were synthesized in the Shanghai GenePharma Co. Ltd.
565 (Shanghai, China). The RNAi and miRNA treatments were performed by feeding dsRNA or
566 miRNA antagomir/agomir through an artificial diet as described previously [50]. Briefly, twenty
567 females at 7 DAE were placed into a glass cylinder (25 × 75 mm) and sealed with two
568 stretched paramembranes. 200 μL of 20% (w:v) sucrose mixed with dsRNA was placed
569 between two paramembranes for feeding. The final ingestion concentrations of ds*DcAKH* and
570 ds*DcAKHR* were 200 ng/μL and 300 ng/μL, respectively. After feeding with dsRNA for 48 h, the
571 treated females were assayed as follows. The ovaries were dissected or qRT-PCR and
572 western blot analysis. Reproductive parameters including the pre-oviposition period,
573 oviposition period, and fecundity were recorded. *C*Las titers in the ovaries were assayed.
574 Ovary morphologies were observed using a Ultra-Depth Three-Dimensional Microscope
575 (VHX-500). Fat bodies were stained with Nile red. TAG levels and glycogen levels were
576 determined. Green fluorescent protein (GFP) was used as a reporter gene. Feeding ds*GFP*
577 was used as the control when psyllids were fed with dsRNA. All the experiments were
578 performed in three replications, and each replication included 15-20 pairs of *D. citri*.

579

580 **Heterologous expression and calcium mobilization assay**

581 The complete ORF of *DcAKHR* was cloned into the expression vector pcDNA3.1$^+$; cloning
582 was confirmed by sequencing (TSINGKE Bio). Endotoxin-free plasmid DNA of the vector was
583 extracted, and all tested peptides were synthesized by Sangon Biotech (Shanghai, China) at a
584 purity >95 % (see Fig. 1B for peptide structures). Chinese hamster ovary (CHO-WTA11) cells
585 supplemented with Gα16 subunit and aequorin were used [51] and transfected with
586 pcDNA3.1$^+$-*DcAKHR* or empty pcDNA3.1$^+$ (negative control) vectors using Lipofectamine
587 2000 (Thermo Fisher Scientifc, Waltham, MA USA). The calcium mobilization assay was
588 performed with slight modification as described by Gui et al. (2017) [52] and Shi et al. (2017)
589 [53]. In brief, the cells were incubated for 3 h in the dark with coelenterazine h (Promega,

590 Madison, WI, USA) 48 h after the transfection. Then, serial dilutions of peptide ligands (10^{-6} to
591 10^{1} μM) were loaded into opaque 96-well plates. Luminescence was measured over 15 s
592 using a SpectraMax i3x Multi Mode Microplate Reader (Molecular Devices). Medium alone
593 was used as a blank control and 100 μM ATP was served as a positive control. Each
594 experiment was repeated three times.
595
596 **JH titer detection**
597 JH titers were assessed using the Insect JH Ⅲ ELISA kit (Shanghai Enzyme-linked
598 Biotechnology Co., Ltd. Shanghai, China) following the manufacturer's protocol.
599
600 **Statistical analysis**
601 All statistical values are presented as means ± SEM. Statistical analyses were performed
602 by GraphPad Prism 8.0 software. Student's *t*-test was used to determine the pairwise
603 comparisons at the following significance levels (*P < 0.05, **P < 0.01, ***P < 0.001). For
604 multiple comparisons, one-way ANOVA with Tukey's Honest Significant Difference tests used
605 to separate means at P < 0.05.
606

607 Acknowledgments

608 This research was supported by the National Natural Science Foundation of China, grant
609 number 32102193, and the Open Competition Program of Ten Major Directions of Agricultural
610 Science and Technology Innovation for the 14th Five-Year Plan of Guangdong Province, grant
611 number 2022SDZG07.
612

613 Author Contributions

614 Conceptualization: Jiayun Li, Paul Holford, George Andrew Charles Beattie, Yurong He, Yijing
615 Cen, Xiaoge Nian.
616 Data curation: Jiayun Li, Shujie Wu, Jielan He, Xiaoge Nian.
617 Formal analysis: Jiayun Li, Xiaoge Nian, Desen Wang.
618 Funding acquisition: Xiaoge Nian, Yurong He, Yijing Cen.
619 Investigation: Jiayun Li, Shujie Wu, Jielan He, Shijian Tan, Xiaoge Nian.

620 Methodology: Jiayun Li, Paul Holford, George Andrew Charles Beattie, Yurong He, Xiaoge
621 Nian, Yijing Cen.
622 Project administration: Xiaoge Nian, Yijing Cen.
623 Resources: Jiayun Li, Shujie Wu, Jielan He, Xiaoge Nian, Yijing Cen.
624 Software: Jiayun Li, Xiaoge Nian, Desen Wang.
625 Supervision: Yurong He, Yijing Cen.
626 Validation: Jiayun Li, Paul Holford, George Andrew Charles Beattie, Xiaoge Nian.
627 Visualization: Jiayun Li, Paul Holford, George Andrew Charles Beattie, Yurong He, Xiaoge
628 Nian, Yijing Cen.
629 Writing-original draft: Jiayun Li, Xiaoge Nian, Yijing Cen.
630 Writing-review & editing: Jiayun Li, Paul Holford, George Andrew Charles Beattie, Xiaoge Nian,
631 Yijing Cen.
632

633 ## Competing interests

634 The authors declare no conflict of interest.
635

636 ## Data Availability Statement

637 The published article includes all data generated or analyzed during this study. The full
638 sequences were submitted to NCBI, accession number: MG550150.1 for *DcAKH*, OR259432
639 for *DcAKHR*, OP251123 for *DcMet*, XM_026820026.1 for *DcKr-h1*, XM_008488883.3 for
640 *DcVg-1-like*, XM_026832896.1 for *DcVg-A1-like* and OP251122 for *DcVgR*.
641

642 ## References

643 [1] Eigenbrode SD, Bosque-Pérez NA, Davis TS. Insect-borne plant pathogens and their
644 vectors: Ecology, evolution, and complex interactions. Annu Rev Entomol. 2018;
645 63:169-191.
646 [2] Mao QZ, Wu Wei, Liao ZF, Li JJ, Jia DS, Zhang XF, et al. Viral pathogens hitchhike with
647 insect sperm for paternal transmission. Nat Commun. 2019; 10:955.
648 [3] Berasategui A, Breitenbach N, García-Lozano M, Pons I, Sailer B, Lanz C, et al. The leaf
649 beetle *Chelymorpha alternans* propagates a plant pathogen in exchange for pupal

650 protection. Curr Biol. 2022; 32:4114-4127.
651 [4] Ray S, Casteel CL. Effector-mediated plant-virus-vector interactions. Plant Cell. 2022;
652 34:1514-1531.
653 [5] Capoor SP, Rao DG, Viswanath SM. *Diaphorina citri* Kuway. A vector of the greening
654 disease of citrus in India. Indian J. Agric. Sci, 1967; 37:572-576.
655 [6] Gottwald TR. Current epidemiological understanding of citrus Huanglongbing. Annu Rev
656 Phytopathol. 2010; 48:119-139.
657 [7] Bové JM. Huanglongbing or yellow shoot, a disease of Gondwanan origin: Will it destroy
658 citrus worldwide? Phytoparasitica. 2014; 42:579-583.
659 [8] da Graça JV, Douhan GW, Halbert SE, Keremane ML, Lee RF, Vidalakis G, et al.
660 Huanglongbing: An overview of a complex pathosystem ravaging the world's citrus. J
661 Integr Plant Biol. 2016; 58:373-387.
662 [9] Fuentes A, Braswell WE, Ruiz-Arce R, Racelis A. Genetic variation and population
663 structure of *Diaphorina citri* using cytochrome oxidase I sequencing. PLoS ONE. 2018;
664 13:e0198399.
665 [10] Beattie GAC. Management of the Asian citrus psyllid in Asia. In: Qureshi JA, Stansly PA
666 (eds) Asian Citrus Psyllid: Biology, Ecology and Management of the Huanglongbing
667 Vector. CAB International, Wallingford, UK. 2020; 179-209.
668 [11] Graham J, Gottwald T, Setamou M. Status of huanglongbing (HLB) outbreaks in Florida,
669 California and Texas. Tropical Plant Pathology. 2020; 45:265-278.
670 [12] Li S, Wu F, Duan Y, Singerman A, Guan Z. Citrus greening: Management strategies and
671 their economic impact. HortScience. 2020; 55:604-612.
672 [13] Pelz-Stelinski KS, Killiny N. Better together: Association with '*Candidatus* Liberibacter
673 asiaticus' increases the reproductive fitness of its insect vector, *Diaphorina citri*
674 (Hemiptera: Liviidae). Ann Entomol Soc Am. 2016; 109:371-376.
675 [14] Ren SL, Li YH, Zhou YT, Xu WM, Cuthbertson AGS, Guo YJ et al. Effects of *Candidatus*
676 Liberibacter asiaticus on the fitness of the vector *Diaphorina citri*. J Appl Microbiol. 2016;
677 121:1718-1726.
678 [15] Wu FN, Qureshi JA, Huang JQ, Fox EGP, Deng XL, Wan FH, et al. Host plant-mediated
679 interactions between '*Candidatus* Liberibacter asiaticus' and its vector *Diaphorina citri*

680 Kuwayama (Hemiptera: Liviidae). J Econ Entomol. 2018; 111:2038-2045.
681 [16] Arrese EL, Soulages JL. Insect fat body: energy, metabolism, and regulation. Annu Rev
682 Entomol. 2010; 55:207-225.
683 [17] Stone JV, Mordue W, Batley KE, Morris HR. Structure of locust adipokinetic hormone, a
684 neurohormone that regulates lipid utilisation during flight. Nature. 1976; 263:207-211.
685 [18] Toprak U. The role of peptide hormones in insect lipid metabolism. Front Physiol. 2020;
686 11:434.
687 [19] Azeez OI, Meintjes R, Chamunorwa JP. Fat body, fat pad and adipose tissues in
688 invertebrates and vertebrates: the nexus. Lipids Health Dis. 2014; 13:71.
689 [20] Gáliková M, Diesner M, Klepsatel P, Hehlert P, Xu Y, Bickmeyer I, et al. Energy
690 homeostasis control in *Drosophila* adipokinetic hormone mutants. Genetics. 2015;
691 201:665-683.
692 [21] Park Y, Kim YJ, Adams ME. Identification of G protein-coupled receptors for *Drosophila*
693 PRXamide peptides, CCAP, corazonin, and AKH supports a theory of ligand-receptor
694 coevolution. Proc Natl Acad Sci U S A. 2002; 99:11423-11428.
695 [22] Staubli F, Jorgensen TJ, Cazzamali G, Williamson M, Lenz C, Sondergaard L, et al.
696 Molecular identification of the insect adipokinetic hormone receptors. Proc Natl Acad Sci
697 U S A. 2002; 99:3446-3451.
698 [23] Ziegler R, Isoe J, Moore W, Riehle MA, Wells MA. The putative AKH receptor of the
699 tobacco hornworm, *Manduca sexta*, and its expression. J Insect Sci. 2011; 11:40.
700 [24] Attardo GM, Benoit JB, Michalkova V, Yang G, Roller L, Bohova J, et al. Analysis of
701 lipolysis underlying lactation in the tsetse fly, *Glossina morsitans*. Insect Biochem Mol Biol.
702 2012; 42:360-370.
703 [25] Konuma T, Morooka N, Nagasawa H, Nagata S. Knockdown of the adipokinetic hormone
704 receptor increases feeding frequency in the two-spotted cricket *Gryllus bimaculatus*.
705 Endocrinology. 2012; 153:3111-3122.
706 [26] Jedlička P, Ernst UR, Votavová A, Hanus R, Valterová I. Gene expression dynamics in
707 major endocrine regulatory pathways along the transition from solitary to social life in a
708 bumblebee, *Bombus terrestris*. Front Physiol. 2016; 7:574.
709 [27] Hou QL, Chen EH, Jiang HB, Wei DD, Gui SH, Wang JJ, et al. Adipokinetic hormone

710 receptor gene identification and its role in triacylglycerol mobilization and sexual behavior
711 in the oriental fruit fly (*Bactrocera dorsalis*). Insect Biochem Mol Biol. 2017; 90:1-13.
712 [28] Lu K, Wang Y, Chen X, Zhang X, Li W, Cheng Y, et al. Adipokinetic Hormone receptor
713 mediates trehalose homeostasis to promote vitellogenin uptake by oocytes in *Nilaparvata*
714 *lugens*. Front Physiol. 2019; 9:1904.
715 [29] Zheng H, Chen C, Liu C, Song Q, Zhou S. Rhythmic change of adipokinetic hormones
716 diurnally regulates locust vitellogenesis and egg development. Insect Mol Biol. 2020;
717 29:283-292.
718 [30] Bartel DP. Metazoan microRNAs. Cell. 2018; 173:20-51.
719 [31] Asgari S. Role of microRNAs in insect host-microorganism interactions. Front Physiol.
720 2011; 2:48.
721 [32] Asgari S. Role of microRNAs in arbovirus/vector interactions. Viruses. 2014;
722 6:3514-3534.
723 [33] Zhang SD, An SH, Hoover K, Li Z, Li XR, Liu, XM, et al. Host miRNAs are involved in
724 hormonal regulation of HaSNPV-triggered climbing behaviour in *Helicoverpa armigera*.
725 Mol Ecol. 2018; 27:459-475.
726 [34] Bryant B, Macdonald W, Raikhel AS. microRNA miR-275 is indispensable for blood
727 digestion and egg development in the mosquito *Aedes aegypti*. Proc Natl Acad Sci U S A.
728 2010; 107:22391-22398.
729 [35] Zhang Y, Zhao Bo, Roy S, Saha TT, Kokoza VA, Li M, et al. microRNA-309 targets the
730 Homeobox gene *SIX4* and controls ovarian development in the mosquito *Aedes aegypti*.
731 Proc Natl Acad Sci U S A. 2016; 113:E4828-4836.
732 [36] Song JS, Zhou ST. Post-transcriptional regulation of insect metamorphosis and
733 oogenesis. Cell Mol Life Sci. 2020; 77:1893-1909.
734 [37] Ling L, Kokoza VA, Zhang C, Aksoy E, Raikhel AS. MicroRNA-277 targets *insulin-like*
735 peptides *7* and *8* to control lipid metabolism and reproduction in *Aedes aegypti*
736 mosquitoes. Proc Natl Acad Sci U S A. 2017; 114:E8017-E8024.
737 [38] Singh R, Linksvayer TA. *Wolbachia*-infected ant colonies have increased reproductive
738 investment and an accelerated life cycle. J Exp Biol. 2020; 223:jeb220079.
739 [39] Grönke S, Mildner A, Fellert S, Tennagels N, Petry S, Müller G, et al. Brummer lipase is

740 an evolutionary conserved fat storage regulator in *Drosophila*. Cell Metab. 2005;
741 1:323-330.
742 [40] Lorenz MW. Adipokinetic hormone inhibits the formation of energy stores and egg
743 production in the cricket *Gryllus bimaculatus*. Comp Biochem Physiol B Biochem Mol Biol.
744 2003; 136:197-206.
745 [41] Lorenz MW, Gäde G. Hormonal regulation of energy metabolism in insects as a driving
746 force for performance. Integr Comp Biol. 2009; 49:380-392.
747 [42] Lindemans M, Liu F, Janssen T, Husson SJ, Mertens I, Gäde G, et al. Adipokinetic
748 hormone signaling through the gonadotropin-releasing hormone receptor modulates
749 egg-laying in *Caenorhabditis elegans*. Proc Natl Acad Sci U S A. 2009; 106:1642-1647.
750 [43] Lucas KJ, Roy S, Ha J, Gervaise AL, Kokoza VA, Raikhel AS. MicroRNA-8 targets the
751 Wingless signaling pathway in the female mosquito fat body to regulate reproductive
752 processes. Proc Natl Acad Sci U S A. 2015; 112:1440-1445.
753 [44] Page RE Jr, Rueppell O, Amdam GV. Genetics of reproduction and regulation of
754 honeybee (*Apis mellifera* L.) social behavior. Annu Rev Genet. 2012; 46:97-119.
755 [45] Lampe L, Jentzsch M, Kierszniowska S, Levashina EA. Metabolic balancing by miR-276
756 shapes the mosquito reproductive cycle and *Plasmodium falciparum* development. Nat
757 Commun. 2019; 10:5634.
758 [46] Roy S, Saha TT, Zou Z, Raikhel AS. Regulatory pathways controlling female insect
759 reproduction. Annu Rev Entomol. 2018; 63:489-511.
760 [47] Lu K, Chen X, Liu WT, Zhang XY, Chen MX, Zhou Q. Nutritional Signaling Regulates
761 Vitellogenin Synthesis and Egg Development through Juvenile Hormone in *Nilaparvata*
762 *lugens* (Stål). Int J Mol Sci. 2016; 17:269.
763 [48] Lu K, Chen X, Liu WT, Zhou Q. TOR pathway-mediated juvenile hormone synthesis
764 regulates nutrient-dependent female reproduction in *Nilaparvata lugens* (Stål). Int J Mol
765 Sci. 2016; 17:438.
766 [49] Hosseinzadeh S, Shams-Bakhsh M, Mann M, Fattah-Hosseini S, Bagheri A, Mehrabadi
767 M, et al. Distribution and variation of bacterial endosymbiont and "*Candidatus*
768 Liberibacter asiaticus" titer in the Huanglongbing insect vector, *Diaphorina citri*
769 Kuwayama. Microb Ecol. 2019; 78:206-222.

770 [50] Yu XD, Killiny N. RNA interference of two glutathione S-transferase genes, *Diaphorina*
771 *citri DcGSTe2* and *DcGSTd1*, increases the susceptibility of Asian citrus psyllid
772 (Hemiptera: Liviidae) to the pesticides fenpropathrin and thiamethoxam. Pest Manag Sci.
773 2018; 74:638-647.
774 [51] Jiang HB, Gui SH, Xu L, Pei YX, Smagghe G, Wang JJ. The short neuropeptide F
775 modulates olfactory sensitivity of *Bactrocera dorsalis* upon starvation. J Insect Physiol.
776 2017; 99:78-85.
777 [52] Gui SH, Jiang HB, Liu XQ, Xu L, Wang JJ. Molecular characterizations of natalisin and its
778 roles in modulating mating in the oriental fruit fly, *Bactrocera dorsalis* (Hendel). Insect Mol
779 Biol. 2017; 26:103-112.
780 [53] Shi Y, Jiang HB, Gui SH, Liu XQ, Pei YX, Xu L, et al. Ecdysis Triggering Hormone
781 Signaling (ETH/ETHR-A) Is Required for the Larva-Larva Ecdysis in *Bactrocera dorsalis*
782 (Diptera: Tephritidae). Front Physiol. 2017; 8:587.
783